Journal Pre-proof



Highly Sensitive Optical Sensor for Hydrogen Gas Based on a Polymer Microcylinder Ring Resonator

Nima Bavili, Timuçin Balkan, Berna Morova, Mustafa Eryürek, Yiğit Uysallı, Sarp Kaya, Alper Kiraz

PII: S0925-4005(20)30153-2

DOI: https://doi.org/10.1016/j.snb.2020.127806

Reference: SNB 127806

To appear in: *Sensors and Actuators: B. Chemical*

Received Date: 20 October 2019

Revised Date: 6 January 2020

Accepted Date: 1 February 2020

Please cite this article as: Bavili N, Balkan T, Morova B, Eryürek M, Uysallı Y, Kaya S, Kiraz A, Highly Sensitive Optical Sensor for Hydrogen Gas Based on a Polymer Microcylinder Ring Resonator, *Sensors and Actuators: B. Chemical* (2020), doi: https://doi.org/10.1016/j.snb.2020.127806

This is a PDF file of an article that has undergone enhancements after acceptance, such as the addition of a cover page and metadata, and formatting for readability, but it is not yet the definitive version of record. This version will undergo additional copyediting, typesetting and review before it is published in its final form, but we are providing this version to give early visibility of the article. Please note that, during the production process, errors may be discovered which could affect the content, and all legal disclaimers that apply to the journal pertain.

© 2020 Published by Elsevier.

Journal Pre-proof

Highly Sensitive Optical Sensor for Hydrogen Gas Based on a Polymer Microcylinder Ring Resonator

Nima Bavili

Department of Physics, Koç University, 34450 Istanbul, Turkey

Timuçin Balkan

Koç University TÜPRAŞ Energy Center (KUTEM), 34450 Istanbul, Turkey

Department of Chemistry, Koç University, 34450 Istanbul, Turkey

Berna Morova

Department of Physics, Koç University, 34450 Istanbul, Turkey

Mustafa Eryürek

TUBITAK BILGEM UEKAE, Gebze, 41470 Kocaeli, Turkey

Yiğit Uysallı

Department of Physics, Koç University, 34450 Istanbul, Turkey

Sarp Kaya

Koç University TÜPRAŞ Energy Center (KUTEM), 34450 Istanbul, Turkey

Department of Chemistry, Koç University, 34450 Istanbul, Turkey

Alper Kiraz*

Department of Physics, Koç University, 34450 Istanbul, Turkey

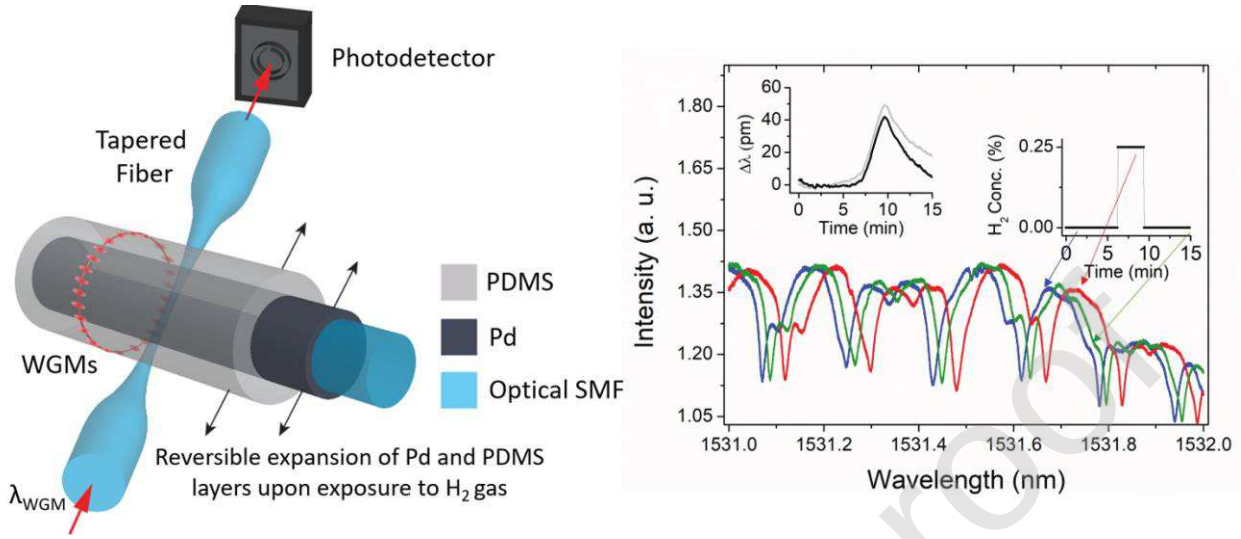
Department of Electrical and Electronics Engineering, Koç University, 34450 Istanbul, Turkey

**Corresponding author Tel: +90 212 338 1701. E-mail address: akiraz@ku.edu.tr*

Journal Pre-proof

Journal Pre-proof

Graphical abstract



Highlights

- Robust, easy-to-fabricate and sensitive hydrogen gas sensor using optical fiber resonators coated with a Pd nanofilm and a PDMS layer is presented
- Sensing mechanism relies on the spectral shifts of the optical whispering gallery modes circulating in PDMS layer observed due to the expansion or contraction of the inner Pd nanofilm
- Maximum spectral shift sensitivity of 140 pm/% H2 and limit of detection of around 60 ppm is demonstrated
- Performance parameters of sensors obtained with amorphous Pd nanofilms and Pd nanofilms annealed in air or nitrogen atmospheres are compared
- Amorphous Pd nanofilms revealed the best performance due to the smaller grains within the film, resulting in faster diffusion and enhanced solubility of H in the Pd layer
- Effects of oxygen gas and humidity on sensor performance were investigated, decrease in sensitivity was observed in the presence of oxygen gas while presence of humidity revealed no significant change in sensor performance

Journal Pre-proof

Journal Pre-proof

ABSTRACT

A highly sensitive platform is demonstrated for hydrogen gas (H_2) sensing based on a polymer microcylinder ring resonator (PMRR) obtained by an optical fiber coated with an inner nanofilm of amorphous palladium (Pd) and an outer polymer layer of polydimethylsiloxane (PDMS) permeable to H_2. The sensing scheme is based on monitoring the spectral shifts of high-quality optical resonances called whispering gallery modes (WGMs) that propagate in the vicinity of the outer rim of the PDMS layer without being affected by the absorption and scattering losses caused by the Pd nanofilm. WGMs are excited by a single-mode tapered optical fiber evanescently coupled to the PMRR. The observed reversible spectral shifts of the WGMs are induced by changes in the diameter of the PDMS layer caused by expansion or contraction of the Pd nanofilm exposed to varying concentrations of H_2. Maximum spectral shift sensitivity of 140 pm/% H_2, a minimum response time of 95 sec, and minimum limit of detection of ~60 ppm were measured for sensors prepared with different thicknesses of the amorphous Pd nanofilm and tested in the H_2 concentration range up to 1%, having nitrogen gas (N_2) as a carrier. Experiments were also conducted with Pd nanofilms annealed in air or N_2 atmosphere after the deposition. In both cases, smaller sensitivities were observed due to the formation of larger grains within the film, resulting in slower diffusion and reduced solubility of H in the Pd layer. The impacts of oxygen gas and humidity on sensor performance were also studied.

Keywords: Hydrogen sensor; Microresonator; Ring resonator; Whispering gallery mode; Palladium; Polydimethylsiloxane

Journal Pre-proof

Journal Pre-proof

1. INTRODUCTION

Hydrogen gas (H_2) is traditionally and widely used in petroleum, chemical and food industries [1]. Recently, it has also received a lot of attention in the energy sector as a promising source of green energy, due to the gradual exhaustion of sources of conventional fossil fuels, pollution resulting from their combustion, and increasing demand for alternative energy sources [2, 3]. Several long-term measures have been adopted in order to increase research and investment in different H_2-related subfields such as production, storage, transportation and detection of H_2 [4, 5]. H_2, with flammability range of 4-75% in the air [6], has a highly explosive nature, so its detection and monitoring play key roles in the hydrogen-related industries.

For the purpose of H_2 detection, several sensing mechanisms have been proposed and some of them have been already commercialized [7]. These include, for example, catalytic [8], thermal conductivity [9], electrochemical [10], resistance-based [11], mechanical [12], acoustic [13] and optical [14-16] detection schemes. Optical detection methods are distinguished from other sensing techniques since the absence of any ignition source makes them safer. In addition, optical detection can be based on different measurement procedures such as reflectance [17], interferometry [18], surface plasmon resonance [19, 20], evanescent field interaction [21], and fiber Bragg gratings [22], which further increases its flexibility for diverse sensing applications.

Optical microresonators have been previously employed in several studies on hydrogen gas sensing. In particular, a silicon-on-insulator ring resonator coated with platinum-doped tungsten oxide was used as a catalytic hydrogen gas sensor [23]. Although a sensitivity of 480 pm/% H_2 in the spectral position of the optical resonances was obtained, the catalytic sensor lacked reversibility. In another study [24], a Pd-coated vertical-cavity surface-emitting laser (VCSEL) was demonstrated, where 52 pm red-shift in optical resonances was measured in a 4% H_2 environment, using the complex VCSEL structure. Photolithographically fabricated Pd-coated SU-8 microdisk resonators [25] and Pd-coated microfiber knot resonators [16] with relatively low Q factors of around 10^3 were also used for H_2 sensing. SU-8 microdisk resonators revealed good spectral shift sensitivities (32 pm/% H_2) due to the mechanical expansion of Pd and, consequently, of the SU-8 microdisk upon exposure to H_2. For the case of the microfiber knot resonator, the

Journal Pre-proof

sensing response was due to the change of Pd refractive index, revealing spectral shift sensitivities around 50 pm/% H_2.

Most of the H_2 detection techniques (both optical and non-optical) reported in the literature to date have employed Pd metal as a sensing material [7] because of its enormous lattice expansion while exposed to H_2. This expansion is due to the formation of a solid solution of Pd and H containing palladium hydride (PdHx), which crystallizes in α and β crystalline phases. Although both α and β phases of the Pd-H system have the same face-centered cubic (fcc) crystalline lattice, they have a huge difference in the lattice expansion value (increase in the lattice constant of Pd before and after the exposure to H_2); lattice expansion value can reach up to 0.13% and 3.47% for α and β phases, respectively [26]. There is an intermediate stage in which both α and β phases exist simultaneously [27, 28].

Phase transitions in pure Pd might cause structural deformations such as cracking and peeling of Pd from the supporting substrate, which may translate into hysteresis in the response of H_2 sensors. Several approaches have been suggested to prevent such mechanical damages. The two main alternatives are using Pd alloys instead of pure metal and application of Pd nanostructures instead of bulk material. For instance, a higher structural durability of sensing materials based on Pd/Ni alloys has been demonstrated in previous studies [14, 29]. Furthermore, reduction/removal of hysteresis effects and faster response of sensors based on nanostructures of Pd have been also reported [14]. It is important to consider the hydrogen-metal interaction independently for the bulk and thin film cases. For instance, a thin film substrate can prevent lattice expansion in the plane of the film and allow only expansion in the perpendicular direction [30]. Furthermore, it has been shown that vacancies, dislocations, and cracks formed during metal coating can act as traps and increase diffusion and solubility of H in the metal. These defects are caused by the fast nature of the coating process [31, 32] and have to be taken into account when designing the layout of the sensor.

In this work, we report fabrication and characterization of a novel and robust optical platform for sensing H_2 based on a polymer microcylinder ring resonator (PMRR) obtained by an optical fiber coated with two functional layers: (i) An inner sensing layer composed of morphology-modified Pd nanofilm (ii) an outer polydimethylsiloxane (PDMS) layer that forms the actual

Journal Pre-proof

optical resonator while allowing for easy penetration of H_2 to the inner sensing layer. Thanks to the good optical properties of PDMS, especially its smooth surface and low absorption cross section in the visible and near-infrared spectral regions, it can host high-quality optical resonances called whispering gallery modes (WGMs) (see Figure 1). In addition to good optical properties, rubbery and elastic characteristic, it has been shown that PDMS has a high permeation to H_2 among other diatomic gases, with almost no H_2-polymer matrix interaction which makes it a perfect choice for this sensor design [33, 34]. The theory of WGMs in cylindrical microresonators is well explained in Ref. [35]. WGMs in optical microresonators are highly sensitive to both the diameter of the resonator, and the refractive indices (RIs) of the resonator and the surrounding medium. In our configuration, changes in concentration of H_2 are detected by observing spectral shifts of the WGMs due to Pd layer expansion or contraction, which subsequently cause an expansion of the outer polymer layer. Similar optical fiber resonator-based refractive index sensors (without outer coatings) that employ spectral shifts of the WGMs as their sensing mechanism have already been presented and fully characterized [36].

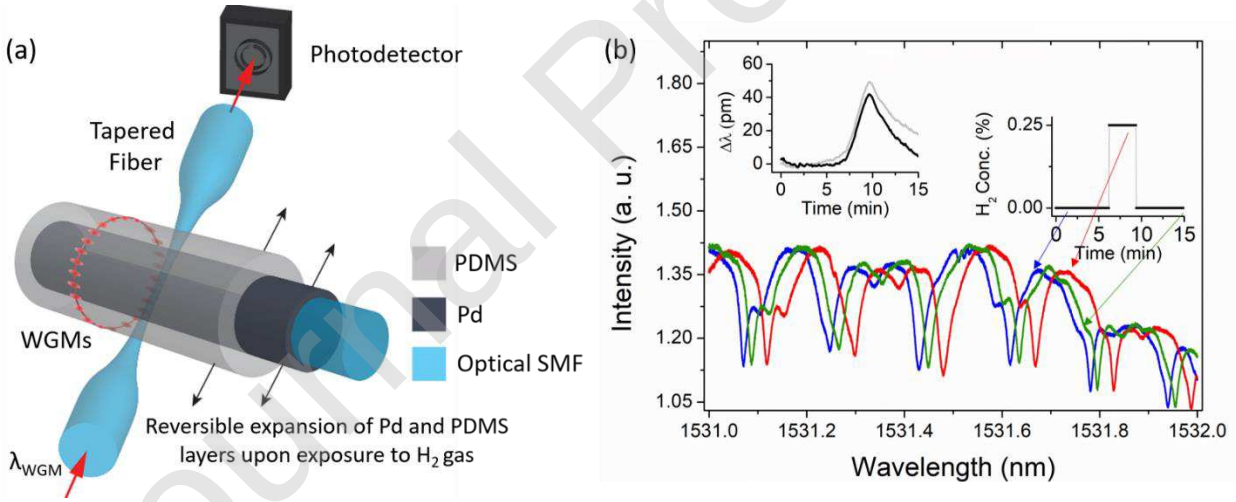


Figure 1. (a) Illustration of the H_2 sensing mechanism. H_2 molecules penetrate the Pd layer through PDMS. Expansion of the Pd layer upon H_2 dissolution then causes an expansion of the PDMS layer and, subsequently, an increase in the optical path length of WGMs circulating near the outer rim of the PDMS layer. Hence, the spectral position of a given WGM shifts to the red end of the spectrum. (b) Reversible spectral shifts in the positions of WGMs recorded upon increase (blue curve to red curve) and decrease (red curve to green curve) in H_2 concentration. The left

Journal Pre-proof

inset shows the time trace of the WGM spectral positions of an exemplary mode before (grey curve) and after (black curve) applying a linear correction (see text for explanation).

We report H_2 sensing below the flammable limit, in the H_2 concentration range of 0.0312 - 1%, exhibiting up to 140 pm/% H_2 sensitivity in the spectral positions of the WGMs together with good reversibility in the sensing response and a limit of detection of ~60 ppm. The reported sensor which combines high sensitivity, good reversibility and low limit of detection achieves highest performance benchmarks among other previous microresonator-based H_2 sensor demonstrations. Furthermore, we investigate the effects of the morphology and composition of the Pd coating on the sensitivity of our optical sensors. In particular, we test amorphous Pd, Pd (II) oxide (PdO) and crystalline Pd nanofilms and show that the application of amorphous Pd nanofilm with defects, e.g., cracks and vacancies, increases the sensitivity of the optical sensor due to the increased diffusion and dissolution of H in the Pd layer. In addition to its good sensing performance, PMRR configuration with amorphous Pd layer improves the sensor repeatability by reducing the risk of peeling off of the Pd nanofilm from the underlying optical fiber following multiple H_2 sensing cycles [14, 25]. In addition, we show that the existence of the O_2 gas in the environment reduces the sensor sensitivity. In contrast, humidity only leads to a background shift without affecting the actual sensitivity to the H_2 gas.

2. MATERIALS AND METHODS

Double-coated PMRRs were prepared from standard single-mode optical fibers (SMFs) with a diameter of 125 ± 0.7 μm (SMF-28-100, Thorlabs) by mechanical stripping of the protective plastic jacket from the fiber and subsequent cleaning of the bare glass surface with isopropyl alcohol (IPA). In order to deposit the Pd film, previously cleaned fibers were fixed and glued between two ring-shaped plexiglass holders with outer and inner diameters of 10 cm and 9 cm, respectively. The coating was performed using RF magnetron sputtering (Vaksis PVD-Handy/2S) in an argon (Ar) atmosphere at room temperature and by rotating the holder. Before the start of the coating process, the base pressure of the sputtering chamber was reduced to 1×10−6 Torr, as this low pressure is necessary to prevent contaminants on the nanofilm.

Journal Pre-proof

During the actual coating, the flow rate of Ar was kept constant at 10 standard cubic centimeters per minute (SCCM) and the RF power was set to 100 W. The Pd target was also pre-cleaned by the rf plasma to prevent contamination during the coating. Sputtering durations up to 4.5 minutes were employed and the fibers were flipped half-way through the process to coat both halves of the fibers (grill configuration) [37]. Using a scanning electron microscope (SEM) imaging (Zeiss Ultra Plus field emission), Pd layer thicknesses were measured to be up to ~100 nm. Since the Pd deposition during the RF sputtering is rather rapid, Pd crystallization is kinetically prevented. As described below, the degree of crystallinity of the Pd film is a key factor in the sensitivity of our sensor configuration. To investigate the effect of crystallinity of Pd coating on H_2 sensing performance, Pd coated fibers were annealed at 500°C or 650°C in the air or in a nitrogen gas (N_2) atmosphere for one hour [38].

After the deposition of the Pd layer, a PDMS polymer layer was added on top of the fiber to form the actual optical ring resonator. PDMS was selected for its good optical properties, flexibility, and inertness and good permeability for H_2 [39]. PDMS layer was added by 7-times repeated dip coating (KSV Nima Multi Vessel Dip Coater) with a coating velocity of 107 mm/min for each repetition (see Figure S5). The parameters of the coating process were adjusted in order to achieve an optimal thickness of the final PDMS layer. Specifically, a thick polymer layer may suppress Pd lattice expansion and reduce H_2 diffusion to the sensing Pd layer, whereas with a thin polymer layer, WGM light might couple to the Pd layer, which leads to optical losses due to absorption and scattering. In our studies, the polymer layer thickness of around 5 μm proved to provide an overall good sensor performance. A 5:1 mixture of the PDMS base and curing agent (Sylgard 184; Dow Corning) was used for the PDMS layer preparation. In addition, toluene was added to the mixture with a ratio of 1:3 to decrease the viscosity of the mixture and, consequently, obtain a uniform polymer layer. These parameters were kept constant for all PMRR-based sensors. After the dip coating process, the fibers were placed vertically at 100°C for around two hours in order to solidify the PDMS layer.

In order to investigate the chemical composition and structure of the Pd coatings, X-ray photoelectron spectroscopy (XPS) and X-ray diffraction (XRD) analyses were performed on Pd nanofilms sputter-coated on flat silica surfaces. XPS measurements (Thermo Scientific, K-Alpha)

Journal Pre-proof

were done using an Al K-α X-ray source and the spectra were energy-calibrated using C 1s peak obtained from advantageous carbon present on the surfaces. A flood gun was used in the measurements to reduce surface charging. XRD investigations (Bruker D8 Advances that uses Cu K-α radiation from a Cu anode) were performed using grazing-incidence geometry.

In the next stage, fiber coated with Pd and PDMS layers was placed in contact with a tapered optical fiber used for coupling of the laser light into the resonator (see Figure 1 for details of the fiber geometry). Both the tapered and coated fibers were fixed and glued to a rectangular chamber. Tapering of the light-coupling fiber was performed by the heat-and-pull method, as reported previously [36]. The tapering length was adjusted to reach the minimal thickness of the tapered fiber of ~3 μm, enabling efficient coupling of light to the PMRR. After mounting the fibers, the chamber was moved to a home-made aluminum enclosure to perform the actual gas sensing experiments. Figure 1 shows exemplary transmission spectra recorded during a gas sensing experiment. Upon an increase in H_2 concentration, a red-shift is observed in the WGMs as a result of the expansion of the PDMS layer, whereas reduction of H_2 concentration to the starting value leads to an almost fully reversible blue-shift of the WGMs.

The schematic of the experimental setup is shown in Figure 2. Similar to our previous work [36], one side of the tapered fiber was coupled to a tunable laser (Santec, TSL-510-Type C, tuning range: 1500–1630 nm, wavelength resolution: 1pm). The power transmitted through the tapered fiber at the given wavelength upon interaction with the PMRR was measured by an InGaAs detector (Thorlabs DET10C/M) and a current amplifier (Stanford Research Systems, SR570) and recorded by a computer. In this experimental configuration, WGMs were observed as dips in the recorded transmission spectra. Figure 1b shows such exemplary transmission spectra exhibiting multiple WGMs with a typical quality factor (Q-factor) of ~50000. Gas tanks with 100% N_2, 99/1% N_2/ H_2, and synthetic air (80/20% N_2/O_2) were connected to the enclosure containing the chamber with the attached fibers. N_2 was chosen as the initial carrier gas (case 1 in Figure 2) as suggested in references [29, 39-42], as its adsorption in both Pd and PDMS is insignificant at room temperature and, thus, it does not interfere with the measurements of H_2 concentration [43]. In addition, for investigating the impact of O_2 gas on sensor performance, experiments were performed by using a mixture of synthetic air and H_2 such that O_2 concentration was fixed at 10%

Journal Pre-proof

for all H_2 concentrations (case 2 in Figure 2). Gas flows into the enclosure were controlled by independent mass flow controllers (Bronkhorst, EL-FLOW) and the gases were mixed at desired ratios before reaching the enclosure. The impact of the humidity was also studied independently by placing a water bubbler in one of the flow controller outlets (case 3 in Figure 2), fixing the ambient humidity in the enclosure to 50%. The temperature and humidity values of the enclosure were continuously monitored by a home-made electronic detector during humidity and synthetic air experiments.

All H_2 sensing measurements were performed at 23°C room temperature and atmospheric pressure. For sensing experiments with N_2, the sensing chamber was first purged with N_2 for at least 30 minutes in order to remove residual water vapor from the sensor environment before initiating the actual measurements. For measurements with synthetic air, synthetic air was employed as the purging gas. During the purging process, a large blue shift of WGMs was observed in most of the fabricated sensors, which corresponded to the sudden decrease in the water content of the polymer layer (Figure S2) [44]. In most of the fabricated sensors, a gradual background shift dependent on the laser light intensity was also observed (Figure S1 in the supp. information). This shift was attributed to the thermal expansion of the PMRR coating due to the absorbed light. In order to reduce or remove this background shift from the recorded transmission spectra, either laser power could be reduced or a mathematical correction could be applied to the spectra [25]. In all experiments presented in this work, we reduced the laser power coupled into the tapered fiber to less than 3 mW. This laser power was five times lower compared to those used in our previous refractometric sensor demonstrations based on optical fiber resonators [25]. In addition, a linear correction was also applied to the time traces of the WGM spectral positions to compensate for the background shift, assuming the shift occurs at a constant rate (see Supp. Info. for the details of the correction procedure). The transmission spectra shown in blue and green colors in Figure 1b illustrate such an exemplary background shift observed between the beginning and the end of a H_2 sensing cycle. The left inset in Figure 1b then shows the time trace of the WGM spectral positions before (gray) and after (black) applying the linear correction procedure.

Journal Pre-proof

3. RESULTS AND DISCUSSIONS

3.1. PMRRs with unannealed Pd nanofilms

We performed systematic sensing experiments, in which we repeatedly increased and decreased the concentration of H_2 in a stepwise fashion, to investigate the sensor performance parameters such as sensitivity and repeatability. We investigated three different Pd sensing layers: (I) unannealed, (II) air-annealed and (III) N_2-annealed. In these experiments N_2 was selected as the carrier gas to rule out the effect of competitive O_2 adsorption on Pd at room temperature. Since the thickness of the Pd nanofilm has a direct impact on the sensitivity of the sensor (see Figure 3), the resonators with similar Pd thicknesses of around 80 nm were selected for comparative analysis of the effects of structural transformation of the Pd nanofilm (see Figure 4). Observed differences in the thickness of the Pd layer could be caused either by different durations of the sputtering processes or by using resonators attached to different locations within the previously mentioned ring-shaped plexiglass holder used during sputtering. In particular, the resonators made of coated PMRRs mounted in the central part of the holder had thicker Pd coatings than those located closer to the edge of the holder. Figure 3 shows SEM images and time traces of WGM spectral shifts of two sensors with unannealed Pd layer thicknesses of ~67 nm (parts (a) and (b)) and 23 nm (parts (c) and (d)). Spectral shift sensitivities of 66 pm/% H_2 and 26 pm/% H_2, respectively, are observed for these two sensors, clearly demonstrating the effect of Pd layer thickness on the sensitivity. On the basis of these findings, the preferred Pd layer thickness for our experiments was chosen in the 50-100 nm range. For reference, a time trace obtained in a control experiment with no Pd layer is also shown in the central inset of Figure 3d. This plot shows that in the absence of the Pd layer, spectral positions of the WGMs are not affected by the H_2 concentrations, hence the adsorption of H_2 into PDMS is negligible under our experimental conditions.

Journal Pre-proof

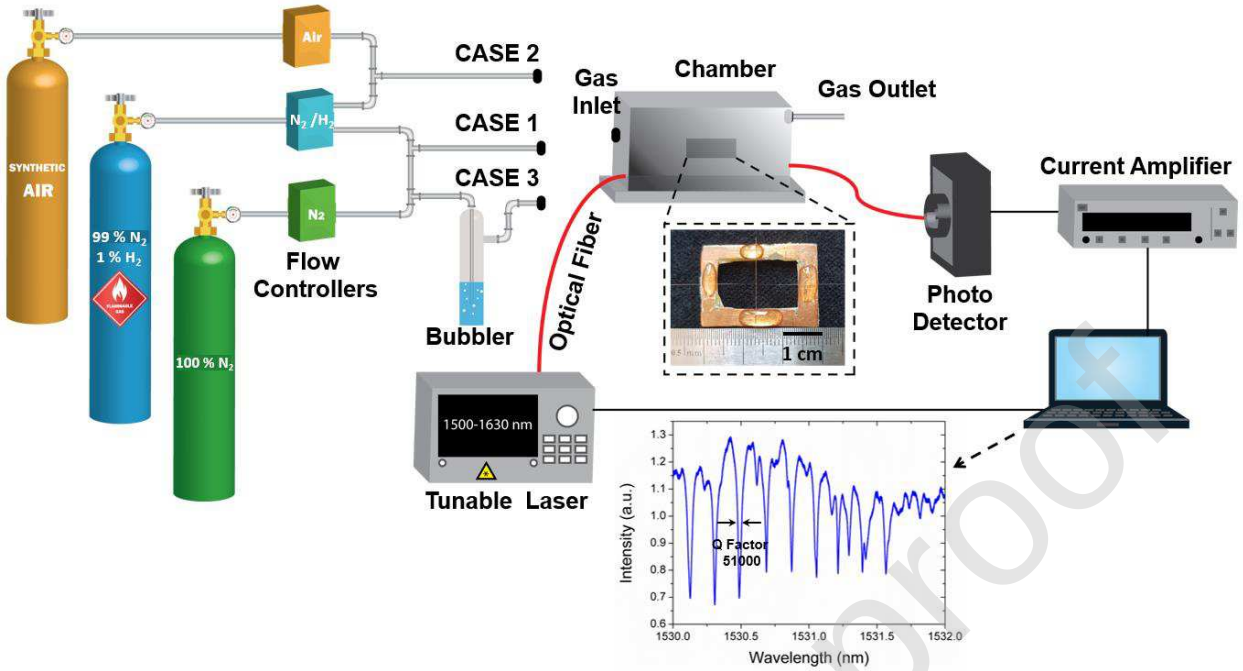


Figure 2. Schematics of the experimental set-up for the detection of H_2 concentration. An exemplary transmission spectrum recorded between 1530 – 1532 nm, exhibiting a WGM with Q-factor of ~51000, is also shown in the inset.

Journal Pre-proof

Journal Pre-proof

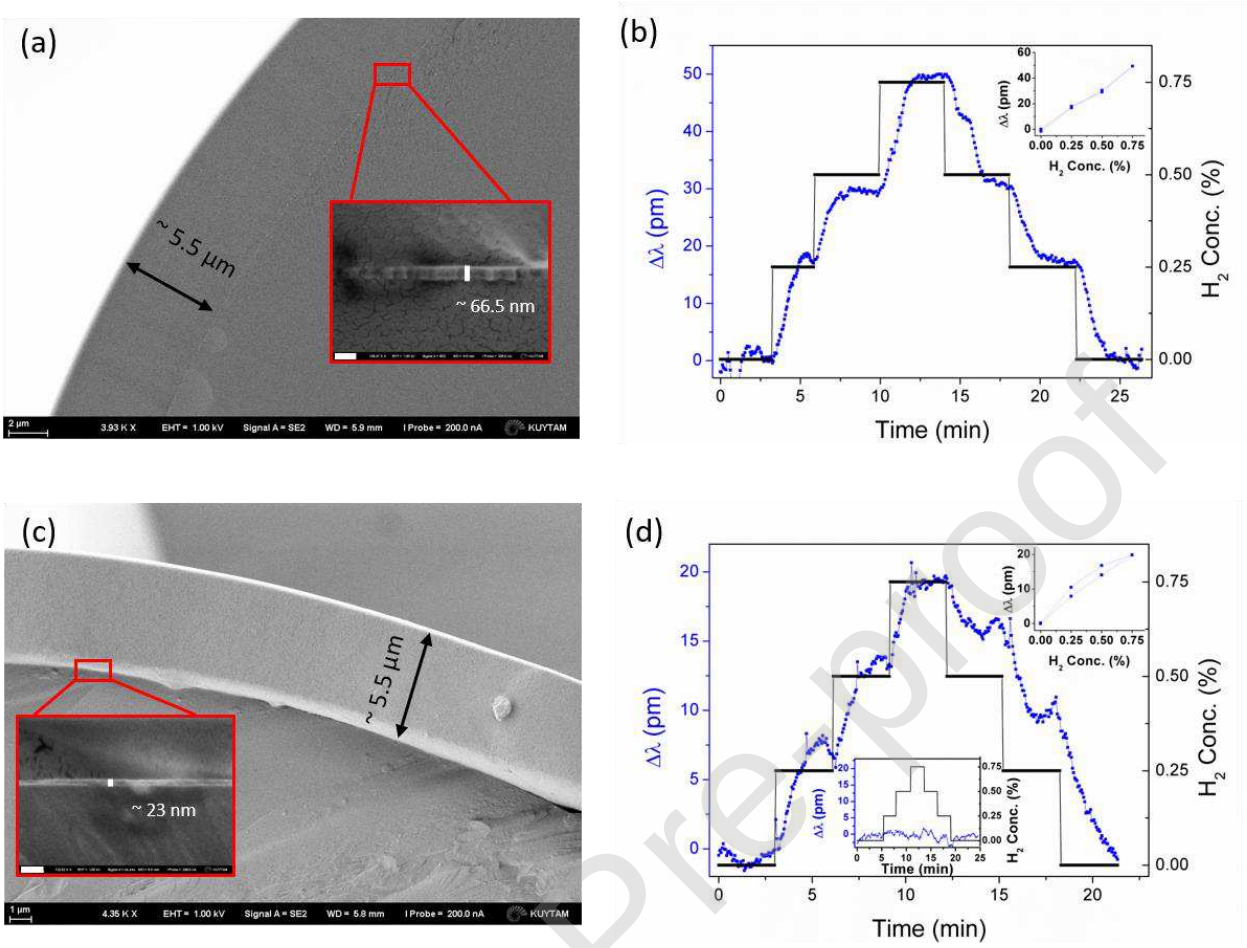


Figure 3. Characterization of the performance of H_2 sensors based on unannealed Pd films. Parts (a) and (c) show cross-sectional SEM images of two PMRRs coated with a similar PDMS thickness but different Pd nanofilm thicknesses. White scale bars shown under the enlarged inset images represent 100 nm. Parts (b) and (d) show time traces of WGM spectral shifts recorded for PMRRs shown in (a) and (c), respectively, while H_2 concentration was changed in a stepwise manner. Blue curves denote the measured WGM spectral shifts, black lines denote the actual H_2 concentrations. Insets in the top right corner of parts (b) and (d) show the sensitivity graphs for the two sensors. An exemplary time trace of WGM spectral shifts recorded during a control experiment with no Pd layer is shown as the central inset in (d)

Pd-H interaction (both in the bulk and in thin films) has been studied extensively and it is well known that it involves two distinct phases called α and β, as well as an intermediate stage where both α and β phases coexist [45]. Upon adsorption and interaction with the Pd surface, H_2 molecules dissociate into two H atoms that subsequently start diffusing into the inner Pd layers, leading to the formation of the initial Pd-H solid solution represented by the α-phase. Further

Journal Pre-proof

increase in the concentration of H causes the formation of the β phase in the Pd-H system (formation of PdH_x) [45]. H-to-Pd atomic fraction (x) is known to be lower than 0.015 for the pure α phase and higher than 0.61 for the pure β phase [26]. The corresponding relative lattice expansions (Δa/a0) for the α- and β-phases are then 0.13% and 3.47%, respectively, with a0 being the lattice constant in the absence of H and Δa being the absolute lattice expansion [26]. For α + β mixed phase, the parameter values lie between $0.015 < x < 0.61$ and $0.13\% < \Delta a/a0 < 3.47\%$ [14]. The corresponding ambient H_2 concentration required for inducing phase transitions in the Pd substrate is highly dependent on the thickness, morphology, and purity of the Pd layer, changing widely between 0.1 to 2% [29, 46].

Changes in the refractive index (Δn) and radius (ΔR) of the PMRR translate into spectral shifts of the WGMs ($\Delta\lambda$) hosted by the resonator. The relationship between these parameters is given as $\Delta\lambda/\lambda=\Delta n/n+\Delta R/R$, where λ, R and n correspond to the WGM wavelength, resonator radius, and resonator refractive index, respectively. For our case, the refractive index change can be ignored because the thickness of the PDMS layer prevents the WGMs from penetrating down to the Pd layer and PDMS itself does not interact significantly with H_2.

Considering an exemplary unannealed PMRR with the measured Pd and PDMS thicknesses of ~66 nm and ~5.5 μm, respectively, as in Figure 3a-b, and the maximum $\Delta\lambda$ value of 18 pm at 0.25% of H_2 concentration, we obtain $\Delta R/R=1.2\times10\text{-}8$. This radius change corresponds to an expansion of approximately 1.2% in the Pd lattice, corresponding to the intermediate α + β phase regime.

3.2. PMRRs with annealed Pd nanofilms

The effects of the thermal annealing of the Pd layer on the sensor performance are illustrated in Figure 4, which shows the time traces of the WGM spectral shifts and the corresponding sensitivity graphs of sensors prepared with unannealed, air-annealed (at two different annealing temperatures) and N_2-annealed PMRRs with similar Pd layer thicknesses. The sensitivity experiments were done with the H_2 concentration increasing and decreasing in 0.25% steps and the maximum concentration value of 0.75% with carrier N_2. As indicated by Figure 4, sensors prepared with air-annealed and N_2-annealed PMRRs show lower spectral shifts compared to the

Journal Pre-proof

unannealed sensors. Specifically, at the H_2 concentration of 0.75%, the reduction in WGM spectral shift is around 37% and 45% for the PMRRs air-annealed at 500°C and 650°C, respectively (see Figure 4a). Similarly, the sensor prepared with N_2-annealing at 500°C shows 33% lower shift at 0.75% H_2 concentration with respect to the unannealed PMRR, as shown in Figure 4b.

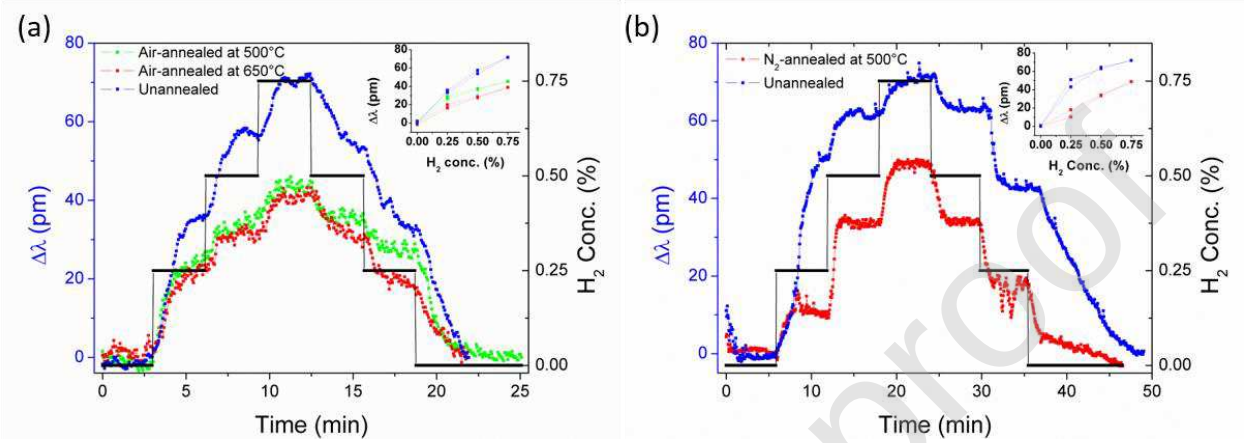


Figure 4. Time traces of WGM spectral shifts recorded during experiments with sensors prepared under different annealing conditions. (a) WGM spectral shifts recorded with an unannealed PMRR (blue curve) and air-annealed PMRRs (green curve – annealing at 500°C, red curve – annealing at 650°C) with the same Pd layer thickness of around 80 nm. (b) WGM spectral shifts recorded with an unannealed PMRR (blue curve) and N_2-annealed PMRR (red curve) with the same Pd layer thickness of around 80 nm. Black lines denote the actual H_2 concentrations. Insets show the sensitivity curves for the corresponding sensors.

3.3. Chemical structure and morphology of annealed and unannealed Pd nanofilms

In order to investigate the changes in the morphology of the Pd surfaces after annealing, SEM images of the actual coated PMRRs were obtained. As seen in Figure 5a, dense cracks and large pores are observed on the unannealed Pd surfaces. This is due to the relatively rapid sputtering process and lower temperatures used during the Pd coating. As shown in Figures 5b and 5c, the disappearance of the cracks and the formation of crystallites are observed in air-annealed Pd surfaces. The increasing size of the grains at the higher annealing temperature is also visible, as it has been previously reported [38]. Similar morphological changes are also seen after N_2-annealing (Figure 5d), except that the size distribution of surface macropores might vary depending on the post-treatment procedure. The lower sensitivity of the annealed substrates can be attributed to the formation of larger PdO and Pd grains for the cases of air-annealing and N_2-

Journal Pre-proof

annealing, respectively. Larger, compact grains result in overall smaller diffusion of H atoms into the Pd matrix. On the other hand, the existence of dense cracks and vacancies in unannealed Pd sputtered surface enhances the diffusion of H atoms and molecules and, thus, results in higher sensitivities.

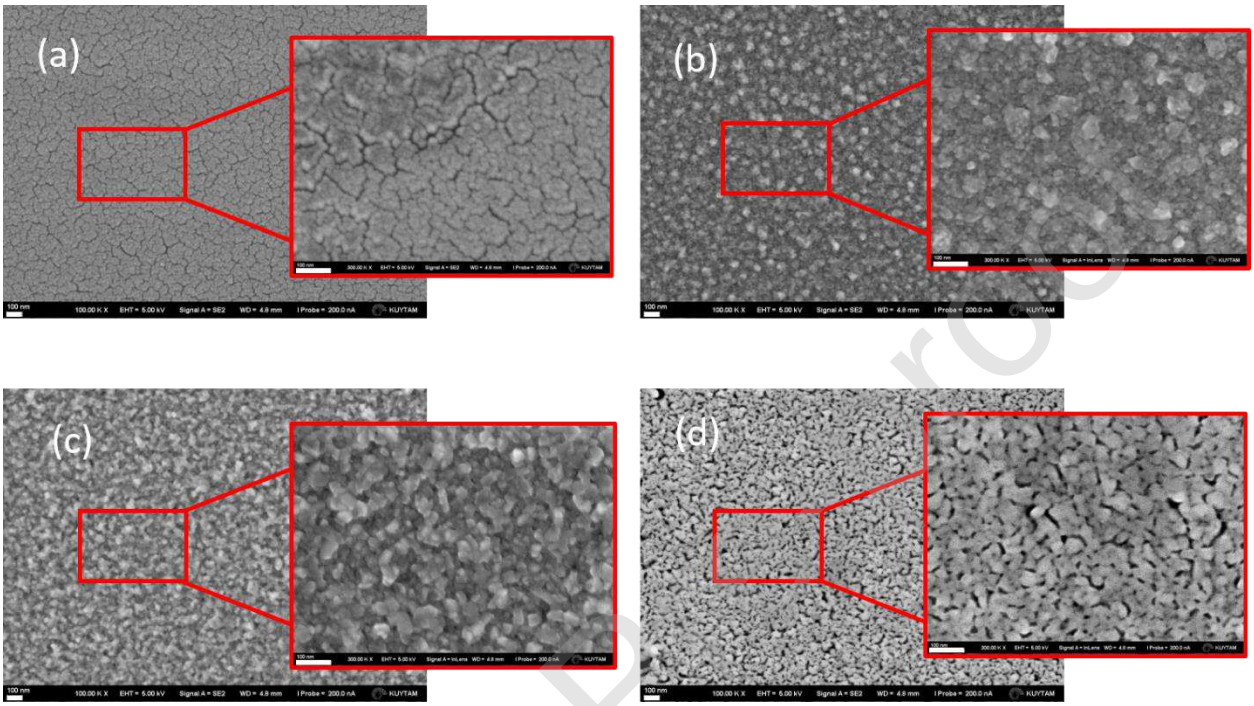


Figure 5. SEM images of (a) an unannealed Pd surface. SEM images of Pd surfaces air-annealed at 500°C (b), air-annealed at 650°C (c), and N_2-annealed at 500°C (d). White scale bars in the images represent 100 nm.

The various Pd coatings used in the sensing experiments were further investigated by XRD and XPS to reveal the structural origins of the observed morphological changes and the chemical state of the Pd surface. The results of these additional surface characterizations are summarized in Figure 6. As it is clear from Figure 6a, the peaks appear at the diffraction angles of 33.90°, 42.10° and 54.90° for air-annealed samples, which suggest the formation of PdO according to JCPDS No. 43-1024. In addition, the diffraction peak at 40.10° can be indexed as PdO according to JCPDS No. 46-1043. As expected, oxidation was not observed for the sample that was annealed under N_2 ambient atmosphere. In agreement with the results of the XRD analysis, XPS analysis also shows the existence of PdO in air-annealed samples. Specifically, unannealed Pd has a 3d5/2 peak located at 335.2 eV that shifts by 2 eV to higher binding energies after air-annealing. This chemical

Journal Pre-proof

shift is a characteristic for PdO formation [47]. A Pd crystal peak at 40.1° only appear at N_2-annealed and air-annealed (500°C) samples. Neither Pd nor PdO peaks appear in the spectrum of the unannealed Pd surface, which confirms the amorphous structure of this substrate [48, 49]. In addition, the width of the Pd 3d XPS peaks reflects the structural order of the sample; the low binding energy tail (binding energies smaller than ~334 eV) observed for the unannealed sample provides evidence of under-coordinated Pd typically present in amorphous structures.

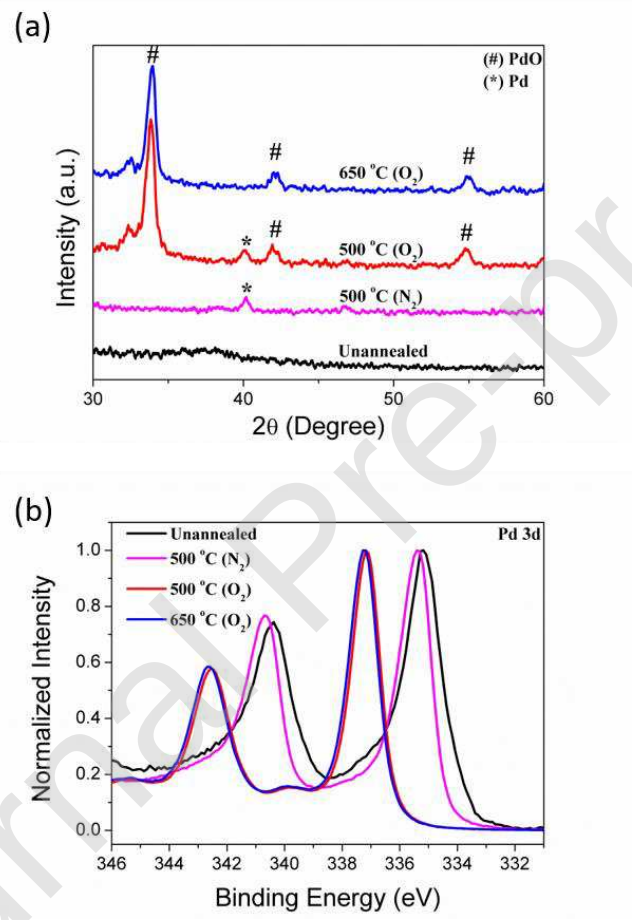


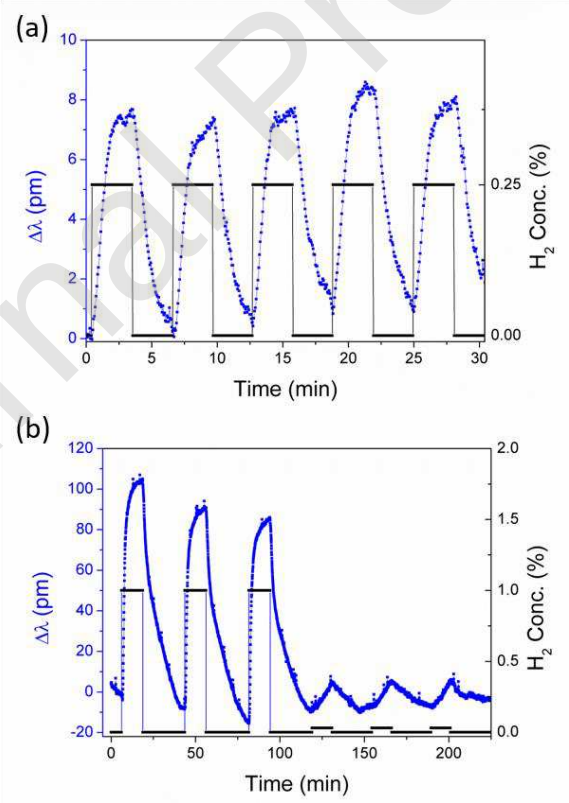
Figure 6. Characterization of the chemical composition and structure of Pd surfaces. (a) XRD patterns recorded for unannealed (black curve), air-annealed (red and blue curves) and N_2-annealed (pink curve) Pd surfaces. (b) XPS patterns recorded for the same surfaces as shown in part (a).

3.4. Repeatability

In order to investigate the repeatability and stability of our H_2 sensors based on PMRRs coated with unannealed (amorphous) Pd nanofilms, experiments with cyclic changes of H_2 concentration were carried out. Figure 7a shows the time trace of WGM spectral shifts obtained during an

Journal Pre-proof

exemplary cyclic experiment, in which H_2 concentration was repeatedly changed between 0 - 0.25%, revealing no significant change in the sensor response at the end of 5 cycles. Figure 7b shows the results of cyclic measurements conducted on another sensor with H_2 concentrations repeatedly changed between 0 - 1% and 0 - 0.0312% (0 - 312 ppm), again revealing no significant change in the sensor performance at both used concentration steps. Figure S3 in the Supp. Info. shows additional data recorded from another sensor, in which two measurements were conducted within a 4-day time interval. Measured sensitivities reported in Figure S3 also show no significant change, indicating the long-time stability of the response of our sensors. Although the absorption and desorption of H from the Pd substrate in both α and β phases of the Pd-H system are reversible and repeatable, some sensors might still suffer from structural deformations such as peeling off and blistering in the Pd surface due to these repeated phase transitions [14]. In our sensor configuration, the outer PDMS layer also acts as a protective layer for the underlying Pd nanofilm and, thus, reduces the risk of these structural damages that might cause a loss of sensitivity.



Journal Pre-proof

Figure 7. Experimental analysis of repeatability and stability of H_2 sensors based on PMRRs coated with unannealed Pd nanofilms. (a) Time trace of WGM spectral shifts recorded during a cyclic experiment with 2500 ppm H_2 concentration steps. (b) Time trace of WGM spectral shifts recorded during a cyclic experiment in which H_2 concentration changed between 0 – 10000 ppm (the first three cycles) and 0 - 312 ppm (the following three cycles). Blue curves denote the measured WGM spectral shifts, black lines denote the actual H_2 concentrations.

3.5. Sensitivity and response time

As presented in the previous paragraphs, there is a trade-off between the sensitivity and response time of the prepared sensors. Thicker Pd nanofilms increase the sensitivity of the H_2 concentration measurements; however, this comes together with an increase in the sensor response time due to the decrease in the surface-to-volume ratio of the Pd nanofilm. The highest sensitivity observed for our sensors was 140 pm/% H_2 with carrier N_2. This particular sensor also exhibited the longest response time of ~4 min (see Figure 8). The response time was measured as the time required for the WGM spectral shift to reach 90% of its total value observed upon a stepwise change of the H_2 concentration in the chamber (see the red dotted lines in Figure 8). In contrast, the sensors presented in Figure 3 have response times of ~100 sec. In the inset of Figure 8, we show the response times measured for different sensors as a function of the sensor sensitivity for H_2 concentration changes from 0 to 0.25%. An increase in the response time with increasing sensitivity is clearly visible in this graph. Response times observed in Figure 7b are 4.52 min and 11.36 min for H_2 concentration changes from 0-1% and 0-0.0312%, respectively. Increase in the sensor response time with decreasing H_2 concentration is consistent with concentration-dependent surface adsorption of H_2 [25, 50].

Journal Pre-proof

Journal Pre-proof

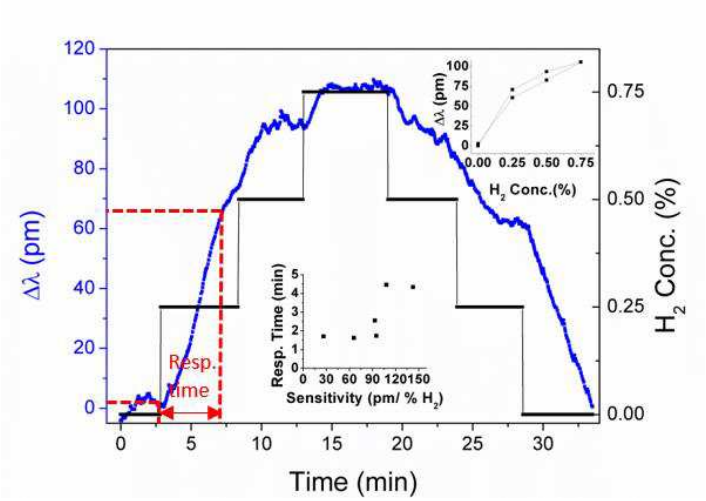


Figure 8. Time trace of WGM spectral shifts recorded during a hysteresis experiment revealing a high spectral shift sensitivity of 140 pm/% H_2 together with a long response time of around 4 min. Blue curve denotes the measured WGM spectral shifts, black line denotes the actual H_2 concentrations. The top right inset shows the spectral shifts corresponding to different H_2 concentrations and the bottom central inset shows the dependence of the response time on the sensitivity recorded for different sensors.

Wavelength stability of our sensors can be found by calculating the standard deviation of the spectral position of a WGM under stable experimental conditions at a constant H_2 concentration. This value was calculated to be 0.39 pm and 0.81 pm for the spectral traces shown in Figures 3b and 8, in which the sensor response plateaus at 0.75% H_2 concentration are clearly observed between t =12-14.30 min and t = 14.8-18.9 min, respectively. Considering the corresponding sensitivities of 66 pm/% H_2 and 140 pm/% H_2 recorded in these experiments, the observed standard deviation values correspond to the detection limits of 59 ppm and 58 ppm for the data presented in Figures 3b and 8, respectively. As depicted in the top right inset of Figure 8, a nonlinear response in the WGM spectral shifts with increasing H_2 concentration was observed for almost all our sensors. In particular, the spectral shift observed upon the change between zero and lowest H_2 concentrations in the given experiment was typically larger than spectral shifts observed at higher H_2 concentrations in the same experiment. We attribute this trend to the transition of the Pd substrate from pure α phase to the state in which both α and β phases coexist in the Pd-H system [16].

Journal Pre-proof

3.6. The impact of oxygen gas and humidity

The effect of the O_2 gas on sensor performance was tackled with experiments employing mixtures of synthetic air and N_2 as the carrier gas. In these experiments, flow controllers were adjusted to provide 10% O_2 concentration at different H_2 concentrations. Figure 9 shows the behavior of an exemplary sensor when H_2 concentration is increased and decreased in a stepwise manner in the presence/absence of ambient O_2 at 10% concentration (red/blue curves). These experiments reveal H_2 sensitivity to drop from 61 pm/%H_2 to 48 pm/%H_2, approximately 20% reduction in the sensitivity, in the presence of 10% O_2 in the environment. This can be attributed to the competitive adsorption of O_2 and H_2. In the absence of O_2, low sticking probability of N_2 at room temperature enhances H_2 sensing behavior. This observation is also consistent with Figure 4 where air-annealed samples showed a reduction in sensitivity by more than 37% due to the changes in the morphology of the Pd surfaces and the formation of PdO, as compared to 33% reduction in sensitivity observed in N_2-annealed samples where PdO was absent. However, despite this deterioration, sensor maintains its capability for H_2 sensing. Figure S4 in the Supp. Info. shows the results of another sensing experiment performed with only one H_2 increasing/decreasing step where sensitivity reduces by around 20% in the presence of 10% O_2.

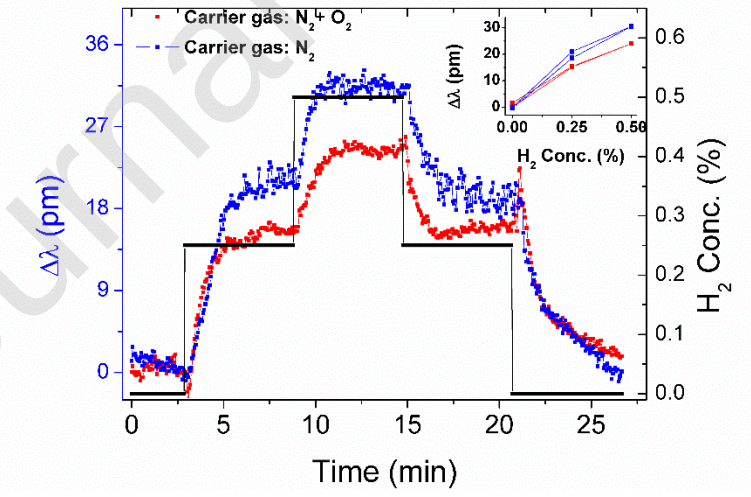


Figure 9. An exemplary time trace of WGM spectral shifts recorded during stepwise increase and decrease of H_2 in the absence (blue curve) and presence of 10% O_2 (red curve) in the carrier gas. 10% O_2 shows around 20% reduction in sensor sensitivity.

Journal Pre-proof

The impact of humidity on the sensor performance was also studied by performing similar stepwise experiments under 50% relative humidity. Figure 10 shows the sensor response to 0.5% H_2 concentration during three consecutive measurements separated by red dotted lines where ambient humidity was changed from 0% to 50% and then from 50% to 0%. In these experiments, the change in humidity only translates to a background shift without significantly affecting the actual shift caused by introduction of H_2 into the chamber. The background shift caused by humidity can be attributed to the interaction between the polymer layer and water (see Figure S2).

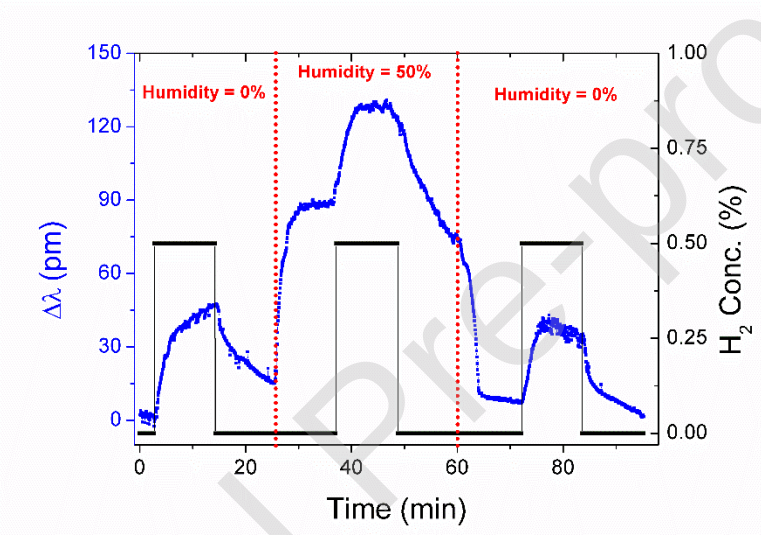


Figure 10: An exemplary time trace of WGM spectral shifts recorded during three consecutive measurements separated by red dotted lines. Initial and final measurements were performed at 0% humidity while the intermediate measurement was performed at 50% humidity. Humidity provides a background shift without affecting the sensing mechanism based on Pd-H interaction.

4. CONCLUSIONS

A novel, compact and easy-to-fabricate platform based on a polymer microcylinder ring resonator has been demonstrated for H_2 sensing. This resonator is double-coated with an inner Pd nanofilm and an outer PDMS polymer layer. The amorphous Pd nanofilm with dense cracks and high porosity acts as the sensing layer that undergoes lattice expansion upon exposure to H_2, while the PDMS layer hosts the optical WGMs and, at the same time, allows for penetration of H_2

Journal Pre-proof

into the Pd layer. Following its lattice expansion, the Pd nanofilm applies strain to the PDMS layer, which subsequently leads to a change in the outer diameter of the resonator that can be monitored in a very precise manner by recording the spectral shifts of the WGMs hosted by the resonator. This spectral shift mechanism is used as the actual probe in the demonstrated gas sensing principle.

Amorphous Pd nanofilms as well as air-annealed or N_2-annealed polycrystalline Pd nanofilms have been tested as sensing layers. Higher sensitivities have been observed for the case of amorphous films due to the presence of smaller grains, increasing the diffusion and dissolution of H in the Pd layer. N_2 was selected as the initial carrier gas to rule out the effect of competitive O_2 adsorption on Pd, however additional experiments were performed with synthetic air and N_2 mixture as a carrier gas of H_2 to measure the deterioration of the sensor due to this adsorption effect. In case of pure N_2 environment, experiments with H_2 sensors based on amorphous Pd nanofilms have revealed a maximum spectral shift sensitivity of ~140 pm/% H_2, a minimum response time of 95 sec, and a minimum limit of detection of ~60 ppm for sensors prepared with different Pd nanofilm thicknesses and tested in the H_2 concentration range of 312 - 10000 ppm. The maximum spectral shift sensitivity of 140 pm/% H_2 together with the observed good reversibility yield our sensor configuration among the best performing ones when compared to other microresonator-based optical H_2 sensors [16, 23-25]. This sensitivity also compares favorably to other optical sensors such as fiber Bragg grating-based H_2 sensors [51]. In addition, the sensitivity and response time could be further optimized by adjusting the thickness of the sensing layer for the desired application parameters. For example, shorter response times could be achieved by coating the PMRRs with even thinner Pd nanofilms. It is important to note that the maximum studied H_2 concentration of 1% does not constitute a fundamental limit for this sensor and higher concentrations can be tested. Short-term and long-term repeatability experiments have also revealed no considerable degradation in the sensor performance within the studied H_2 concentration range. To this end, the outer PDMS layer plays an important role by reducing the risk of peeling off of the Pd nanofilm from the surface of the silica fiber. Besides serving as a highly sensitive platform for H_2 sensing, the demonstrated configuration also has a good potential to be employed as a tool for sensitive probing of metal-gas interactions [16, 31, 52].

Journal Pre-proof

Adding 10% O_2 to the carrier gas showed around 20% reduction in sensor sensitivity as a result of competitive O_2 adsorption on Pd at room temperature. Further experiments were also performed to study the effect of humidity on the sensor performance. Change in humidity only resulted in a background shift in the spectral positions of the WGMs without significantly affecting the actual shift caused by H-Pd interaction.

Declaration of interests

The authors declare that they have no known competing financial interests or personal relationships that could have appeared to influence the work reported in this paper.

ACKNOWLEDGMENT

This work was supported by TÜBİTAK (Grant No. 115F446). We thank Alexandr Jonáš for proofreading the manuscript. The authors thank KUYTAM for the characterization measurements. S. Kaya and T. Balkan would also like to thank TARLA for the collaborative research support.

REFERENCES

[1] Ramachandran, R. and R.K. Menon, An overview of industrial uses of hydrogen. International Journal of Hydrogen Energy, 1998. 23(7): p. 593-598.

[2] Schlapbach, L. and A. Züttel, Hydrogen-storage materials for mobile applications, in Materials for sustainable energy: a collection of peer-reviewed research and review articles from nature publishing group. 2011, World Scientific. p. 265-270.

[3] Dresselhaus, M. and I. Thomas, Alternative energy technologies. Nature, 2001. 414(6861): p. 332.

Journal Pre-proof

[4] Hosseini, S.E. and M.A. Wahid, Hydrogen production from renewable and sustainable energy resources: promising green energy carrier for clean development. Renewable and Sustainable Energy Reviews, 2016. 57: p. 850-866.

[5] Behling, N., M.C. Williams, and S. Managi, Fuel cells and the hydrogen revolution: Analysis of a strategic plan in Japan. Economic Analysis and Policy, 2015. 48: p. 204-221.

[6] Seader, J., J.J. Siirola, and S.D. Barnicki, Perry's chemical engineer's handbook. Perry's Chemical Engineers' Handbook, 1997.

[7] Hübert, T., et al., Hydrogen sensors–a review. Sensors and Actuators B: Chemical, 2011. 157(2): p. 329-352.

[8] Han, C.-H., et al., Catalytic combustion type hydrogen gas sensor using TiO2 and UV-LED. Sensors and Actuators B: Chemical, 2007. 125(1): p. 224-228.

[9] Simon, I. and M. Arndt, Thermal and gas-sensing properties of a micromachined thermal conductivity sensor for the detection of hydrogen in automotive applications. Sensors and Actuators A: Physical, 2002. 97: p. 104-108.

[10] Korotcenkov, G., S.D. Han, and J.R. Stetter, Review of electrochemical hydrogen sensors. Chemical reviews, 2009. 109(3): p. 1402-1433.

[11] Tomchenko, A.A., et al., Semiconducting metal oxide sensor array for the selective detection of combustion gases. Sensors and Actuators B: Chemical, 2003. 93(1-3): p. 126-134.

[12] Chou, Y.-I., H.-C. Chiang, and C.-C. Wang, Study on Pd functionalization of microcantilever for hydrogen detection promotion. Sensors and Actuators B: Chemical, 2008. 129(1): p. 72-78.

[13] Dong, S., et al., Sound-resonance hydrogen sensor. Applied physics letters, 2003. 82(25): p. 4590-4592.

[14] Noh, J.-S., J.M. Lee, and W. Lee, Low-dimensional palladium nanostructures for fast and reliable hydrogen gas detection. Sensors, 2011. 11(1): p. 825-851.

[15] Shao, J., et al., A New Hydrogen Sensor Based on SNS Fiber Interferometer with Pd/WO3 Coating. Sensors, 2017. 17(9): p. 2144.

[16] Wu, X., F. Gu, and H. Zeng, Palladium-coated silica microfiber knots for enhanced hydrogen sensing. IEEE Photonics Technology Letters, 2015. 27(11): p. 1228-1231.

[17] Butler, M.A., Micromirror optical-fiber hydrogen sensor. Sensors and actuators B: Chemical, 1994. 22(2): p. 155-163.

Journal Pre-proof

[18] Maciak, E. and Z. Opilski, Transition metal oxides covered Pd film for optical H2 gas detection. Thin Solid Films, 2007. 515(23): p. 8351-8355.

[19] Bevenot, X., et al., Surface plasmon resonance hydrogen sensor using an optical fibre. Measurement Science and Technology, 2001. 13(1): p. 118.

[20] Tittl, A., et al., Palladium-based plasmonic perfect absorber in the visible wavelength range and its application to hydrogen sensing. Nano letters, 2011. 11(10): p. 4366-4369.

[21] Tabib-Azar, M., et al., Highly sensitive hydrogen sensors using palladium coated fiber optics with exposed cores and evanescent field interactions. Sensors and actuators B: Chemical, 1999. 56(1-2): p. 158-163.

[22] Sutapun, B., M. Tabib-Azar, and A. Kazemi, Pd-coated elastooptic fiber optic Bragg grating sensors for multiplexed hydrogen sensing. Sensors and Actuators B: Chemical, 1999. 60(1): p. 27-34.

[23] Yebo, N.A., et al., Silicon-on-insulator (SOI) ring resonator-based integrated optical hydrogen sensor. IEEE photonics technology letters, 2009. 21(14): p. 960-962.

[24] Griffin, B.G., et al., Hydrogen detection using a functionalized photonic crystal vertical cavity laser. IEEE Journal of Quantum Electronics, 2011. 48(2): p. 160-168.

[25] Eryürek, M., et al., Optical sensor for hydrogen gas based on a palladium-coated polymer microresonator. Sensors and Actuators B: Chemical, 2015. 212: p. 78-83.

[26] Kim, K.R., et al., Suppression of phase transitions in Pd thin films by insertion of a Ti buffer layer. Journal of materials science, 2011. 46(6): p. 1597-1601.

[27] Alefeld, G. and J. Völkl. Hydrogen in metals I-Basic properties. in Berlin and New York, Springer-Verlag (Topics in Applied Physics. Volume 28), 1978. 442 p.(For individual items see A79-16057 to A79-16061). 1978.

[28] Kalli, K., A. Othonos, and C. Christofidès, Characterization of reflectivity inversion, α-and β-phase transitions and nanostructure formation in hydrogen activated thin Pd films on silicon based substrates. Journal of applied physics, 2002. 91(6): p. 3829-3840.

[29] Lee, E., et al., Hysteresis behavior of electrical resistance in Pd thin films during the process of absorption and desorption of hydrogen gas. international journal of hydrogen energy, 2010. 35(13): p. 6984-6991.

[30] Miceli, P., et al., Anomalous lattice expansion of metal-hydrogen thin films. Journal of Materials Research, 1991. 6(5): p. 964-968.

Journal Pre-proof

[31] Pundt, A. and R. Kirchheim, Hydrogen in metals: microstructural aspects. Annu. Rev. Mater. Res., 2006. 36: p. 555-608.

[32] Flanagan, T.B. and W. Oates, The palladium-hydrogen system. Annual Review of Materials Science, 1991. 21(1): p. 269-304.

[33] Merkel, T., et al., Gas sorption, diffusion, and permeation in poly (dimethylsiloxane). Journal of Polymer Science Part B: Polymer Physics, 2000. 38(3): p. 415-434.

[34] Sadrzadeh, M., K. Shahidi, and T. Mohammadi, Synthesis and gas permeation properties of a single layer PDMS membrane. Journal of applied polymer science, 2010. 117(1): p. 33-48.

[35] Sumetsky, M., Mode localization and the Q-factor of a cylindrical microresonator. Optics letters, 2010. 35(14): p. 2385-2387.

[36] Eryürek, M., et al., Liquid refractometric sensors based on optical fiber resonators. Sensors and Actuators A: Physical, 2017. 265: p. 161-167.

[37] Eryürek, M., Optofluidic Sensing with Optical Microresonators. 2018.

[38] Samavat, F., et al., Effect of Annealing Temperature on the Optical Properties of Palladium Thin Film. Open Journal of Physical Chemistry, 2012. 2(02): p. 103.

[39] Lee, J., et al., Highly mobile palladium thin films on an elastomeric substrate: Nanogap-based hydrogen gas sensors. Angewandte Chemie International Edition, 2011. 50(23): p. 5301-5305.

[40] Monzón-Hernández, D., D. Luna-Moreno, and D. Martínez-Escobar, Fast response fiber optic hydrogen sensor based on palladium and gold nano-layers. Sensors and Actuators B: Chemical, 2009. 136(2): p. 562-566.

[41] She, X., et al., Pd films on soft substrates: a visual, high-contrast and low-cost optical hydrogen sensor. Light: Science & Applications, 2019. 8(1): p. 4.

[42] Favier, F., et al., Hydrogen sensors and switches from electrodeposited palladium mesowire arrays. Science, 2001. 293(5538): p. 2227-2231.

[43] Miyazaki, E., I. Kojima, and S. Kojima, Chemisorption of molecular nitrogen on palladium surfaces at and above room temperature. Langmuir, 1985. 1(2): p. 264-266.

[44] Eryürek, M., et al., Integrated humidity sensor based on SU-8 polymer microdisk microresonator. Sensors and Actuators B: Chemical, 2017. 242: p. 1115-1120.

Journal Pre-proof

[45] Kumar, M.K., M.R. Rao, and S. Ramaprabhu, Structural, morphological and hydrogen sensing studies on pulsed laser deposited nanostructured palladium thin films. Journal of Physics D: Applied Physics, 2006. 39(13): p. 2791.

[46] Zhao, Z., et al., All-optical hydrogen sensor based on a high alloy content palladium thin film. Sensors and Actuators B: Chemical, 2006. 113(1): p. 532-538.

[47] Brun, M., A. Berthet, and J. Bertolini, XPS, AES and Auger parameter of Pd and PdO. Journal of electron spectroscopy and related phenomena, 1999. 104(1-3): p. 55-60.

[48] Ferhat-Hamida, Z., et al., The chemical state of palladium in alkene and acetylene oxidation: A study by XRD, electron microscopy and TD-DTG analysis. Applied Catalysis B: Environmental, 2001. 29(3): p. 195-205.

[49] Reddy, G.K., et al., Understanding the chemical state of palladium during the direct NO decomposition–influence of pretreatment environment and reaction temperature. RSC Advances, 2017. 7(32): p. 19645-19655.

[50] Zhao, Z., et al., All-optical hydrogen-sensing materials based on tailored palladium alloy thin films. Analytical chemistry, 2004. 76(21): p. 6321-6326.

[51] Zhang, Y.-n., et al., Recent advancements in optical fiber hydrogen sensors. Sensors and Actuators B: Chemical, 2017. 244: p. 393-416.

[52] Pundt, A., Hydrogen in nano-sized metals. Advanced Engineering Materials, 2004. 6(1-2): p. 11-21.

Nima Bavili was born in Tabriz in 1989. He received his B.S. degree from Tabriz University, Physics Department in 2012 and his M.Sc. degree from Istanbul Technical University (ITU), Physics Engineering Program in 2015. He joined Koç University Optofluidics and Nano-Optics Research Laboratory in July 2016 to pursue his Ph.D. education.

Timuçin Balkan received his B.S. in Chemistry from Uludağ University in 2008, M.S and Ph.D. degrees in Polymer Science and Technology from İstanbul Technical University. Between 2017 and 2018 he worked as a postdoctoral associate at Chemistry in Bilkent University. He has been working as a researcher at Koç University, Tüpraş Energy Center since 2018.

Journal Pre-proof

Berna Morova has received her B.S., M.S. and Ph.D. degrees in Physics Engineering from Istanbul Technical University. Between the years of 2010 – 2017, she worked as a Research Assistant in the same department. During her Ph.D., she studied on interactions of high-energy shaped laser beams with transparent materials. In 2017, Berna Morova joined Koç University Optofluidics and Nano-Optics Research Laboratory as a post-doctoral researcher and her studies mainly focus on ultrafast lasers, imaging techniques, microfabrication, and microfluidics. In 2019, she also joined Koç University Research Center for Translational Medicine (KUTTAM) Cellular and Molecular Imaging Core's technical team as a post-doctoral researcher.

Mustafa Eryürek was born in Razgrad, Bulgaria in 1987. He received his B.S. degree from Bilkent University, Department of Physics. He received his M.S. and Ph.D. degrees from Koç University, Department of Optoelectronics and Photonics Engineering in 2013; and Department of Physics in 2018, respectively. While in Koç University, he worked mainly on optical microresonator sensors, their fabrication, and characterization. In 2018, he joined UEKAE (National Research Institute of Electronics and Cryptology) in Kocaeli, Turkey as a Senior Researcher, where he is currently working on development of high-power lasers.

Yiğit Uysallı was born in Turkey in 1989. He received his B.S. degree in Physics from Koç University in 2012 where he also worked as the leader of SPIE and OSA chapters. He completed his M.S. degree in Physics at Middle East Technical University in 2016. Currently he is working as a Ph.D. student in Optofluidics and Nano-Optics Research Laboratory in Koç University.

Sarp Kaya received his Ph.D. in Physical Chemistry in 2007 after completing his studies on ultrathin metal oxide layers at Fritz Haber Institute of the Max Plank Society and Humboldt University, Berlin-Germany. During his post-doctoral studies at Stanford University (2007-2010) and following activities as a research scientist at SLAC National Accelerator Laboratory (2010-2013) and Joint Center of Artificial Photosynthesis (JCAP), USA, he heavily utilized synchrotron radiation for surface and interface investigations. In 2013, he joined Koç University where his

Journal Pre-proof

group has been conducting active research in electrical, photochemical, photoelectrochemical, and thermochemical energy conversion. He is interested in every aspects of chemical bond formation with surface and interfaces.

Alper Kiraz received his B.S. degree in electrical-electronics engineering from Bilkent University in 1998, M.S. and Ph.D. degrees in electrical and computer engineering from the University of California, Santa Barbara in 2000 and 2002, respectively. Between 2002 and 2004 he worked as a post-doctoral associate at the institute for physical chemistry in the Ludwig-Maximilians University and received Alexander von Humboldt fellowship. He joined the department of physics of Koç University as an assistant professor in 2004. Currently, he is a professor in the same department. His research interests include optofluidics, single molecule spectroscopy/microscopy, and optical manipulation. Main applications targeted by his research are the development of novel biological and chemical sensors, optofluidic-based renewable energy solutions, and biomedical instruments. He is a member of OSA and SPIE.

Journal Pre-proof

View publication stats